



Nano rutile TiO₂ catalysed synthesis of (E)-4-(2-(1-(4-chlorophenyl)-1H-phenanthro[9,10-d]imidazol-2-yl)vinyl)-N,N-dimethylaniline and its interaction with super paramagnetic nanoparticles

Journal:	<i>RSC Advances</i>
Manuscript ID:	RA-ART-09-2014-010686.R2
Article Type:	Paper
Date Submitted by the Author:	07-Nov-2014
Complete List of Authors:	Thanikachalam, Venugopal; Annamalai University, Chemistry Arunpandiyan, Anandan; Annamalai university, chemistry Jayabharathi, Jayaraman; Annamalai University, Chemistry Karunakaran, C. ; Annamalai University, Chemistry Ramanathan, Periyasamy; Annamalai university, chemistry

Nano rutile TiO₂ catalysed synthesis of (E)-4-(2-(1-(4-chlorophenyl)-1H-phenanthro[9,10-d]imidazol-2-yl)vinyl)-N,N-dimethylaniline and its interaction with super paramagnetic nanoparticles

V. Thanikachalam^{*}, A. Arunpandiyan, J. Jayabharathi, C. Karunakaran, P. Ramanathan

Department of Chemistry, Annamalai University, Annamalainagar 608 002, Tamilnadu, India.

* Address for correspondence

Dr. V. Thanikachalam
Professor of Chemistry
Department of Chemistry
Annamalai University
Annamalainagar 608 002
Tamilnadu, India.
Tel: +91 9443940735
E-mail: vtchalam2005@yahoo.com

Nano rutile TiO₂ catalysed synthesis of (E)-4-(2-(1-(4-chlorophenyl)-1H-phenanthro[9,10-d]imidazol-2-yl)vinyl)-N,N-dimethylaniline and its interaction with super paramagnetic nanoparticles

V. Thanikachalam*, A. Arunpandiyam, J. Jayabharathi, C. Karunakaran, P. Ramanathan

Department of Chemistry, Annamalai University, Annamalainagar 608 002, Tamilnadu, India.

Abstract

Synthesis of (E)-4-(2-(1-(4-chlorophenyl)-1H-phenanthro[9,10-d]imidazol-2-yl)vinyl)-N,N-dimethylaniline (CPPIVI) has been carried out using TiO₂ (R) as catalyst under solvent free condition and characterized by NMR spectral studies. The catalyst was characterized by scanning electron microscopy (SEM) and X-ray diffractometry (XRD). The catalyst is reusable with satisfactory results. The synthesised phosphated styrylimidazole (PSI) and phosphated styrylimidazole bound magnetic nanoparticles (PSIMN) were characterized using SEM, transmission electron microscopy (TEM), energy dispersive X-ray spectroscopy (EDS), XRD and Fourier-transform infrared spectroscopy (FT-IR). The intensities of absorption and emission maxima are of the following order: PSIMN > PSI > CPPIVI. Conductance and VSM measurements were also carried out. The lifetime of the excited states of PSIMN, PSI and CPPIVI have been obtained. The prototropic study of CPPIVI has also been made at different concentrations.

Keywords: TiO₂ (R); PSIMN; FT-IR; SEM; TEM; EDS; XRD.

1. Introduction

Arylimidazoles play important role in materials science and medicinal chemistry due to their optoelectronic properties and high thermal stabilities [1-6]. Substituted imidazoles are extensively used as glucagon receptors [7], antibacterial [8], anti-allergic [9], analgesic [10] and antitumor [11] agents and also as pesticides [12]. Many of the reported synthetic protocols for imidazoles [13-24] suffer from disadvantages such as use of toxic catalysts chlorinated organic solvents, acidic conditions, etc., Thus development of a new catalyst under solvent free condition is essential to overcome these shortcomings and to fulfill milder reaction condition, higher yield and reusability of catalyst. Titanium dioxide finds widespread industrial applications [25-29] and its utility has been extended to the photodegradation of pesticides [30] and carcinogenic dyes [31, 32]. From the synthetic point of view, titanium dioxide has been used as a potential green, inexpensive, mild and recyclable heterogeneous Lewis acid catalyst in organic transformations including synthesis of benzimidazoles [33-39].

The main function of phosphorus is in the formation of bones and teeth. It is crucial for the production of ATP to store energy, works with B vitamins and assists in the contraction of muscles, functioning of kidneys, regulation of heart beat, nerve conduction etc., [40]. Therefore, the synthesis of phosphated styrylimidazole is of our interest. The nanoparticles of iron oxides have been extensively exploited as materials of choice for ferrofluids, high-density information storage, magnetic resonance imaging (MRI), drug delivery, labelling, etc., [41-48]. Phosphoric acid is used as the complexing agent to form phosphated styrylimidazole (PSI) which binds with Fe_2O_3 . The development of biocompatible nano sized drug delivery systems such as magnetic iron oxide nanoparticles for specific targeting of therapeutics is the focus of medical research. An important advantage of nano iron oxide carriers is the possibility for detecting these nanoparticles after treatment with common imaging techniques like x-ray-tomography, magnetorelaxometry and MRI [48].

In continuation of our efforts to develop green and solvent-free synthetic methodologies [49], herein is reported for the first time, a simple one-pot synthesis of styryl phenanthrimidazoles in good yield using sol-gel synthesised nano titanium dioxide as an inexpensive heterogeneous and recyclable non-toxic catalyst under solvent free condition. The photophysical characteristics of the newly synthesised styrylimidazole, phosphated styrylimidazole and phosphated styrylimidazole bound magnetic nanoparticles were investigated. Drug molecules invariably contain nitrogen and the activity of drug depends on the electron density at nitrogen. pH of the medium alters the electron density at nitrogen and hence it is thought worthwhile to probe the prototropic mechanism of CPPIVI also; PSI and PSIMN are unlikely to be stable in acedic pH.

2. Experimental

2.1. Materials and measurements

Phenanthroquinone, *p*-chloroaniline, 4-(4-(dimethylamino) styryl)benzaldehyde and all other reagents have been purchased from Sigma-aldrich. NMR spectra were recorded on Bruker 400 MHz NMR spectrometer and the mass spectra were obtained using an Agilent LCMS VL SD in electron ionization mode. The UV-vis and photoluminescence spectra were recorded with Perkin Elmer Lambda 35 UV-vis spectrophotometer and PerkinElmer LS55 fluorescence spectrometer, respectively. Cyclic voltammetry (CV) and Fluorescence lifetime measurements were carried out with CHI 630A potentiostat electrochemical analyzer and Horiba Fluorocube-01-NL lifetime system with nano LED as the excitation source and TBX-PS as detector, respectively. The PL quantum yields were measured by comparing fluorescence intensities of a standard sample, coumarin 46 and theoretical calculations were performed using Gaussian-03 program [50]. TEM analysis was carried out using JEOL JEM 2100 high resolution transmission electron microscope (HR-TEM) with an accelerating voltage of 200 KV. XRD patterns were recorded for the centrifuged and dried samples using

X-ray Rigaku diffractometer with Cu K_{α} source (30 kV, 100 mA), at a scan speed of 3.0000 deg/min, step width of 0.1000 deg, in a 2θ range of 20-80°. The energy dispersive X-ray (EDS) spectra were recorded with a JEOL JSM-5610 scanning electron microscope (SEM) equipped with back electron (BE) detector and EDX. The sample was placed on an adhesive carbon slice supported on copper stubs and coated with 10 nm thick gold using JEOL JFC-1600 auto fine coater prior to measurement. Magnetic measurements were made at room temperature with a Lakeshore vibrating sample magnetometer.

2.2. Synthesis of nanocrystalline TiO_2 (R) by sol- gel method

The TiO_2 (R) nanocrystal were prepared by sol- gel hydrolysis of titanium(IV) isopropoxide, followed by calcination. About 1ml titanium isopropoxide (Merck, 97%) was dissolved in 20 ml isopropyl alcohol (Merck, 95%) under stirring. The solution was dropped slowly into 10 ml distilled water and the pH was adjusted to 2, the formed white sol-gel hydrous oxide was stirred vigorously for 4 hours at room temperature and then allowed to age overnight. The solid was centrifuged and was redispersed in ethanol to minimize agglomeration. The resulting material was filtered, dried and calcinated upto 800 °C for 2 h. The sample were characterized by x-ray diffraction (XRD) and transmission electron microscopy (TEM) and it is found that high acidity favor for the formation of rutile phase TiO_2 [50,51].

2.3. Synthesis of (E)-4-(2-(1-(4-chlorophenyl)-1H-phenanthro[9,10-d]imidazol-2-yl)vinyl)-N,N-dimethylaniline (CPPIVI)

A mixture of 4-(4-(dimethylamino) styryl)benzaldehyde (1 mmol), phenanthrene-9,10-dione (1 mmol), p- chloroaniline (1 mmol) and ammonium acetate (1 mmol) with TiO_2 (1 mol%) as catalyst was stirred at 120 °C with continuous stirring with a bar magnet. The progress of the reaction was monitored by TLC. After completion of the reaction, 10 ml ethyl acetate was added to the reaction mixture and shaken well to dissolve the organic components

and the mass filtered to separate out TiO_2 and the residue was washed with ethyl acetate. The solid residue of TiO_2 was further washed with hot acetone and then dried up. The product was purified by column chromatography using benzene: ethyl acetate (9:1) as the eluent. The newly synthesised phenanthrimidazole have been characterised by ^1H and ^{13}C NMR and mass (MS) spectra. Yield: 82%, M.p. 248 °C, Anal. calcd. for $\text{C}_{31}\text{H}_{24}\text{N}_3\text{Cl}$: C, 78.55; H, 5.10; N, 8.87. Found: C, 78.28; H, 4.93; N, 8.64. ^1H NMR (400 MHz, CDCl_3): δ 2.96 (s, 6H), 6.23 (s, 2H), 8.39 (s, 1H), 7.49 (s, 1H), 7.53 (s, 1H), 6.46 (d, 1H), 7.89 (d, 1H), 8.86 (d, $J = 8.4\text{Hz}$, 1H), 7.30 (d, $J = 7.2\text{Hz}$, 1H), 7.38 (d, $J = 6.4\text{Hz}$, 1H), 7.09 (q, 1H), 8.72 (q, 3H), 7.60-7.69 (m, 5H). ^{13}C NMR (400 MHz, CDCl_3): δ 40.29, 109.19, 111.48, 112.06, 112.17, 120.72, 121.79, 122.84, 123.14, 123.66, 124.08, 125.12, 125.51, 126.26, 126.97, 127.19, 128.18, 128.30, 128.42, 128.98, 129.85, 130.16, 130.22, 135.64, 137.83, 139.40, 144.30, 145.39, 150.68, 151.07. MS: m/z 474 [M+].

2.4. Synthesis of phosphated styrylimidazole (PSI)

About 1 mmol syrupy phosphoric acid was added to 1 mmol of styrylimidazole in ethanol. The reaction mixture was stirred under room temperature for 1 h. The pale yellow precipitate of phosphated styrylimidazole was washed with ethanol and dried at 110 °C.

2.5. Synthesis of Fe_2O_3 – phosphated styrylimidazole (PSIMN)

About 1 mmol phosphated styrylimidazole in dimethyl sulphoxide was added to 1 mmol of Fe_2O_3 nanoparticles suspended in dimethyl sulphoxide under constant stirring for 3 h. The solid was filtered, washed with dimethyl sulphoxide and dried at 110 °C.

3. Result and discussion

3.1. Characterization of nano TiO_2 (R)

Nanocrystalline rutile TiO_2 obtained by sol–gel method has been characterized by XRD, SEM and energy dispersive X - ray, UV–visible diffuse reflectance (DRS) and solid state photoluminescence spectroscopies. The crystalline phase, average crystalline size (20.4 nm)

and surface area ($51.7 \text{ m}^2/\text{g}$) have been determined by powder XRD (Figure S1). The SEM image (Figure S1) reveals agglomeration of the synthesized nanoparticles. UV-visible DRS (Figure S2) provide the band gap as 3.19 eV. The observed slightly larger band gap is because of the smaller size of the nanoparticles. Quantum confinement effect increases the band gap energy [51]. The PL spectrum (Figure S2) shows emissions at 411, 450, 482 and 530 nm. These emissions are due to trap electrons and oxygen vacancies [52].

3.2. Rutile TiO_2 catalysed synthesis

The (E)-4-(2-(1-(4-chlorophenyl)-1H-phenanthro[9,10-d]imidazol-2-yl)vinyl)-N,N-dimethyl aniline was synthesized using nanoparticulate $\text{TiO}_2(\text{R})$ as catalyst under solvent free conditions; 1 mol % of rutile TiO_2 was used as catalyst at 120°C (Table S1) to get maximum yield (82%) at 30 min. The reaction mechanism and yield are given as supporting information (Figure S3 and S4).

3.3. Characterization of nano Fe_2O_3 – CPPIVI

The synthesized styrylimidazole was phosphated and bound to nano Fe_2O_3 . Figure 1 display the powder diffraction pattern of the phosphated styrylimidazole bound magnetic nanoparticles. The recorded XRD is in agreement with that of maghemite cubic Fe_2O_3 with unit cell length as 0.8352 nm. The peaks at $30.2, 35.7, 43.3, 53.7, 57.3$ and 62.9° correspond to 220, 311, 400, 422, 511 and 440 planes, respectively [JCPDS card no. 39-1346]. The mean crystallite size (L) of the imidazole bound nanoparticles is 30.3 nm and the calculated surface area is $50.58 \text{ m}^2/\text{g}$. The TEM image (Figure 1) confirms they are nanoparticles and the measured crystallite size agrees with that obtained by XRD. The SEM images of phosphated imidazole bound Fe_2O_3 nanoparticle and phosphated imidazole are shown in Figures S5a & S5b, respectively. The EDX spectrum of phosphated imidazole bound Fe_2O_3 nanoparticles and phosphated imidazole are shown in Figures S6a and S6b, respectively. They display the

presence of carbon, nitrogen, phosphorous along with iron. This shows the binding of phosphated imidazole with Fe₂O₃ nanoparticles.

Magnetic hysteresis curves recorded at room temperature for cubic Fe₂O₃ and PSIMN are presented in Figure 2. The hysteresis loops exhibit ferromagnetic behavior, with saturation magnetization (M_S) of 31.4 and 17.62 emu g⁻¹, coercivity (H_C) of 140 and 11.8 Oe and remanant magnetization (M_R) of 5.6 and 0.2 emu g⁻¹, respectively. In the present study, M_S value for the PSIMN is much lower than for the cubic Fe₂O₃ precursor. The low Fe₂O₃ content in PSIMN is the reason for this result. The FT-IR spectra of phosphated imidazole bound Fe₂O₃ nanoparticles, phosphated imidazole, imidazole and Fe₂O₃ nanoparticles are shown in Figure S7 and the prominent frequencies are displayed in Table 1. The frequency around 1600 cm⁻¹ corresponds to C=N function of imidazole, phosphated imidazole and phosphated imidazole bound Fe₂O₃ nanoparticles. The peak around 3375 cm⁻¹ corresponds to \geq C-H in imidazole, phosphated imidazole and phosphated imidazole bound Fe₂O₃ nanoparticles. The peak at \sim 748 cm⁻¹ is likely due to the aromatic C-H stretching. The frequencies at 1080 and 1099 cm⁻¹ are assigned to the phosphate moiety in phosphated imidazole and phosphated imidazole bound Fe₂O₃ nanoparticles. The frequencies at 1647 and 1631 cm⁻¹ are assigned to Fe-O stretching vibration in phosphated imidazole bound Fe₂O₃ and Fe₂O₃ nanoparticles, respectively. The Fe-O stretching vibration of Fe₂O₃ nanoparticles is shifted from 1631 to 1647 cm⁻¹ and this may be due to the binding of imidazole with the superparamagnetic nanoparticles through oxygen of Fe₂O₃ and the binding interaction is shown in Figure 3. Further evidence for the formation of phosphated imidazole bound Fe₂O₃ nanoparticles has been obtained through conductometric measurements. The conductance of imidazole, phosphated imidazole and phosphated imidazole bound Fe₂O₃ in dimethyl sulfoxide is of the order: CPPIVI (128 μ S cm⁻¹) < PSI (130 μ S cm⁻¹) < PSIMN (134 μ S cm⁻¹). Attachment of phosphate enhances the conductance of imidazole through the release of H⁺.

Binding of phosphated imidazole with Fe₂O₃ further increases the conductance. Based on these results the attachment of Fe₂O₃ with phosphated imidazole is shown in Figure 3.

The optical properties of imidazole, phosphated imidazole and phosphated imidazole bound Fe₂O₃ nanoparticles have been studied by electronic spectroscopy. The spectra are shown in Figure 4. The intensities of absorption and emission maxima increases in the following order: PSIMN > PSI > CPPIVI. This observation shows that the interaction of phosphated imidazole with Fe₂O₃ lowers the energy level of the valence band of Fe₂O₃ (Figure S8). A relatively small energy gap between the lowest internal charge transfer states and the locally excited states leads to increase of the contribution of π , π^* character to the wave function of the charge transfer states. This causes lowering of energy with respect to a pure charge transfer state resulting in red shift of the emission.

3.4. Lifetime analysis

The fluorescence decays of imidazole, phosphated imidazole and phosphated imidazole bound Fe₂O₃ follow bi exponential kinetics. The decay curves are shown in Figure 5. The bi exponential decay follows the equation, $S(t) = a_1e^{-t/\tau_1} + a_2e^{-t/\tau_2}$, where a_i and τ_i are amplitudes and time constants of the i^{th} (=1,2) exponential component. The calculated τ_{ave} values are in nanoseconds, displayed in Table 2. This indicates the formation of phosphated imidazole and phosphated imidazole bound Fe₂O₃ nanoparticles. The observed emission lifetime (τ) is indicative of the fact that the styryl phenanthrimidazole interacts with nano Fe₂O₃ through linkage. The determined radiative (k_r) and nonradiative (k_{nr}) rate constants are displayed in Table 2. The radiative emission of PSIMN is larger than those of CPPIVI and PSI. The life time studies reveal that the electron is transferred from the excited CPPIVI to Fe₂O₃ nanoparticles. The rate constant for electron transfer (k_{et}) can be calculated by using the equation, $k_{\text{et}} = 1/\tau_{\text{ads}} - 1/\tau$ and the calculated value of k_{et} is listed in Table 2. The electron transfer efficiency is obtained using the equation, $E\% = (1 - \tau_{\text{PSIMN}}/\tau_{\text{CPPIVI}}) \times 100$.

3.5. Prototropic reactions of CPPIVI

The absorption and emission spectra of (E)-4-(2-(1-(4-chlorophenyl)-1H-phenanthro[9,10-d]imidazol-2-yl)vinyl)-N,N-dimethylaniline (CPPIVI) at different acid concentrations have been studied and the prototropic equilibrium are shown in Figure 6 (Table 3). At [TFA] = 0.04 M in cyclohexane, H₂SO₄ = 0.06 M in dichloromethane and pH = 0.3 in water, the absorption maximum (253 nm) of neutral CPPIVI is blue-shifted to 243 nm and red-shifted to 340 nm with two isosbestic points (Figure 7a) indicating the two-species monocation (MC1 and MC2) are in equilibrium.

The fluorescence maxima of neutral CPPIVI (501 nm) at low acid concentration is blue shifted to 440 nm when excited at 250 nm and on excitation at 335 nm it is red shifted to 520 nm (Figure 7b). The fluorescence intensity at 440 nm in cyclohexane is weak and so the quantum yield could not be measured but it is maximum in dichloromethane (0.48) and minimum in water (0.15). The quantum yield at longer wavelength is maximum in cyclohexane (0.35). In order to support the experimental results (Table 4), quantum-mechanical calculations [53] were carried out on two monocations (MC1 formed by protonation of -NMe₂ group and MC2 obtained by the protonation -N= atom) and a dication (DC formed by protonation of both monocations). The electronic spectral studies confirmed the presence of two monocations. The protonation at -NMe₂ group ($-\overset{\oplus}{\text{N}}\text{HMe}_2$) induces $\pi \rightarrow \pi^*$ transition leading to a blue shift and addition of a proton at -N= atom leads to a red shifted absorption due to $n \rightarrow \pi^*$ transition. The fluorescence spectral analysis also supports the same conclusion. Therefore the blue shifted both absorption (~ 243 nm) and emission (440 nm) bands can be assigned to the monocation (MC1) whereas the red shifted absorption (340 nm) and emission (520 nm) bands are assigned to the monocation (MC2). The dihedral angles (ϕ & θ) between the nitrogen atom and the adjacent aromatic ring (ϕ) as well as between the N,N-dimethylaminostyryl and phenanthrimidazole ring (θ) for CPPIVI,

monocations (MC1 & MC2) and a dication (DC) are displayed in Table 4. The dihedral angle (ϕ) for neutral CPPIVI is (-0.3°), MC1 (5.20°) and MC2 (2.1°) is very small. The dihedral angle (θ) between the lone pair electrons on the $-\text{NMe}_2$ group and the styryl ring affect the spectral properties of the species. In MC1, the large dihedral angle ($\theta = 98^\circ$) and non availability of lone pair on the $-\overset{\oplus}{\text{N}}\text{HMe}_2$ group are responsible for large blue shift [54] whereas the large red shift of MC2 relative to the neutral CPPIVI could be attributed to the presence of the resonance structure MC2 (Figure 6) which can be substantiated by the small dihedral angle (θ) (0.6°) and smaller bond lengths connecting the styryl ring and nitrogen of the $-\text{NMe}_2$ (C–N, 1.2 \AA) and styryl ring and carbon of phenanthrimidazole moiety (C–C, 1.3 \AA) [55-57].

In non-polar solvents, MC2 is more stable than MC1 (103 kJ mol^{-1}) but the dipole moment of MC1 (10.9 D) in the ground state is very large in comparison to that of MC2 (4.2 D). Thus the proportion of a highly polar MC1 will be very small in non-polar solvents in the ground state. In polar solvents MC1 becomes more stable than MC2 by 69 kJ mol^{-1} in the ground state due to very large dipolar stabilization energy and thus its proportion in the polar solvent is increased. Thus, the very small quantum yield of MC1 in non-polar solvent and that of MC2 in polar solvent can be explained. This finding is also supported by the absorbances (A) of MC1 and MC2 in cyclohexane ($A_{\text{MC1}} = 0.50$ & $A_{\text{MC2}} = 1.30$) and in water ($A_{\text{MC1}} = 0.61$ & $A = 0.18$). The decreased quantum yield of MC1 in water relative to that in dichloromethane may be due to solvent induced fluorescence quenching or increase of non-radiative emission [58].

Further increasing the acid concentration in dichloromethane and at $H_0 = 4$ in aqueous medium, the absorption maximum (245 nm) is red shifted with respect to that of MC1 and blue shifted with respect to MC2 with two isosbestic wavelengths and the observed new peak at 245 nm may be due to the formation of dication (DC). This also confirms the existence of

MC1 and MC2. Under similar experimental conditions the fluorescence spectra was recorded. The observed peaks at 423 (MC1), 462 (MC2) and 439 (DC) indicate the presence of both DC–MC1 and DC–MC2 equilibria [58]. Though two monocations are formed, only one pK_a value (2.30) is obtained for the monocation – neutral equilibrium which is larger than that of 2- phenylbenzoxazole (0.0) [55] and smaller than that of N,N-dimethylaniline (4.22) [59]. For 2-phenylbenzoxazole, the protonation occurs at –N= atom whereas in N,N-dimethylaniline, the protonation takes place at –NMe₂ group. The discrepancy can be explained as follows. From Table 4, it is clear that both –NMe₂ and phenanthroimidazole moieties in neutral CPPIVI are nearly coplanar with the styryl ring. Therefore the charge flow from –NMe₂ group to –N= atom of the heterocyclic moiety will increase, i.e. the charge density at –NMe₂ group will decrease and increase of the same at –N= atom. This is supported by the increase of charge density at –N= atom (-0.18) and decrease of charge density at –NMe₂ (-0.21) group in neutral moiety compared with charge density of –N= atom (-0.1294) of 2-phenylbenzoxazole and charge density of –NMe₂ (-0.2866) group of N,N-dimethylaniline, respectively. Due to this charge flow, the pK_a value will be larger than 2-phenylbenzoxazole and smaller than N,N-dimethylaniline. Similar to monocation – neutral equilibria, the pK_a for dication – monocation equilibrium in aqueous medium has been determined using absorption data and is found to be -1.7.

4. Conclusion

We synthesized (E)-4-(2-(1-(4-chlorophenyl)-1H-phenanthro[9,10-d]imidazol-2-yl)viny)-N,N-dimethylaniline using sol-gel synthesized rutile TiO₂ nanocrystals as catalyst. The synthesized phosphated imidazole was bound to Fe₂O₃ nanoparticles and was characterized by SEM, TEM, EDX, XRD, VSM, FT-IR, UV-Vis absorption, emission and lifetime spectral studies. The mean crystallite size of the imidazole bound nanoparticles is 30.3 nm. The shift of Fe-O stretching vibration of from 1631 cm⁻¹ to 1647 cm⁻¹ conforms binding of imidazole

with the superparamagnetic nanoparticles through oxygen of Fe_2O_3 . The intensities of absorption and emission maxima increase in the following order: PSIMN > PSI > CPPIVI. The conductance of the samples in dimethyl sulfoxide is of the order: CPPIVI < PSI < PSIMN. The life time studies also confirmed the formation of PSIMN. The blue shifted absorption and fluorescence bands correspond to the monocation (MC1) whereas the red shifted absorption and fluorescence bands arise out of the monocation (MC2).

5. Acknowledgments

One of the authors Prof. J. Jayabharathi is thankful to DST (No. SR/S1/IC-73/2010), DRDO (NRB-213/MAT/10-11), UGC (F. No. 36-21/2008 (SR)) and CSIR (NO 3732/NS-EMRII) for providing funds to this research study.

References

- [1] N.S. Hush, Distance dependence of electron transfer rates, *Coord. Chem. Rev.* 64 (1985) 135-157.
- [2] R.A. Marcus, Relation between Charge Transfer Absorption and Fluorescence Spectra and the Inverted Region, *J. Phys. Chem.* 93 (1989) 3078-3086.
- [3] I.R. Gould, R.H. Young, R.E. Moody and S. Farid, Contact and solvent-separated geminate radical ion pairs in electron-transfer photochemistry, *J. Phys. Chem.* 95 (1991) 2068-2080.
- [4] I.R. Gould, D. Noukakis, L. Gomez-Jahn, R.H. Young, J.L. Goodman and S. Farid, Radiative and nonradiative electron transfer in contact radical-ion pairs, *J. Chem. Phys.* 176 (1993) 439-456.
- [5] J. Cortes, H. Heitele and J. Jortner, Band-shape analysis of the charge-transfer fluorescence in barrelene-based electron donor-acceptor compounds, *J. Phys. Chem.* 98 (1994) 2527-2536.
- [6] R.S. Mulliken and W.B. Person, *Molecular Complexes: A Lecture and Reprint Volume*, VCH, Weinheim, (1969).
- [7] S.E. deLaszlo, C. Hacker, B. Li, D. Kim, M. Maccoss, N. Mantle, J.V. Pivnichny, L. Colwell, G.E. Koch, M.A. Cascieri and W.K. Hagmann, Potent, orally absorbed glucagon receptor antagonists, *Bioorg. Med. Chem. Lett.* 9 (1999) 641-646.
- [8] M. Antolini, A. Bozzoli, C. Ghiron, G. Kennedy, T. Rossi and A. Ursini, Analogues of 4,5-bis(3,5-dichlorophenyl)-2-trifluoromethyl-1H-imidazole as potential antibacterial agents, *Bioorg. Med. Chem. Lett.* 9 (1999) 1023-1028.
- [9] J. W. Black, G. J. Durant, J. C. Emmett and C. R. Ganellin, Sulphur-methylene isosterism in the development of metiamide, a new histamine H₂-receptor antagonist, *Nature*, 248 (1974) 65-67.

- [10] Ü. Uçucu, N. G. Karaburun and İ. Işıkdag, Synthesis and analgesic activity of some 1-benzyl-2-substituted-4,5-diphenyl-1H-imidazole derivatives, *Il Farmaco*, 56 (2001) 285-290.
- [11] L. Wang, K.W. Woods, Q. Li, K.J. Barr, R.W. McCroskey, S.M. Hannick, L. Gherke, R.B. Credo, Y.H. Hui, K. Marsh, R. Warner, J.Y. Lee, N. Zielinski-Mozng, D. Frost, S.H. Rosenberg and H.L. Sham, Potent, orally active heterocycle-based combretastatin A-4 analogues: synthesis, structure-activity relationship, pharmacokinetics, and in vivo antitumor activity evaluation, *J. Med. Chem.* 45 (2002) 1697-1711.
- [12] T. Maier, R. Schmierer, K. Bauer, H. Bieringer, H. Buerstell and B. Sachse, US Patent 4820335, *Chem. Abstr.* 11 (1989) 1949w.
- [13] S.A. Siddiqui, U. C. Narkhede, S. S. Palimkar, T. Daniel, R. J. Lahoti and K. V. Srinivasan, Room temperature ionic liquid promoted improved and rapid synthesis of 2,4,5-triaryl imidazoles from aryl aldehydes and 1,2-diketones or α -hydroxyketone, *Tetrahedron*, 61 (2005) 3539-3546; (b) M. M. Heravi, M. Zakeri, N. Karimi, M. Saeedi, H. A. Oskooie and N. T. Hosieni, Acidic ionic liquid $[(\text{CH}_2)_4\text{SO}_3\text{HMIM}][\text{HSO}_4]$: a green media for the simple and straightforward synthesis of 2, 4, 5-trisubstituted imidazoles, *Synth. Commun.* 40 (2010) 1998-2006.
- [14] (a) J. Wang, R. Mason, D. VanDerveer, K. Feng and X.R. Bu, Convenient Preparation of a Novel Class of Imidazo[1,5-*a*]pyridines: Decisive Role by Ammonium Acetate in Chemoselectivity, *J. Org. Chem.* 68 (2003) 5415-5418; (b) S. Sarshar, D. Siev and M.M. Mjalli, Imidazole libraries on solid support, *Tetrahedron Lett.* 37 (1996) 835-838; (c) T.F. Gallagher, G.L. Seibel, S. Kassis, J.T. Laydon, M.J. Blumenthal, J.C. Lee, D. Lee, J.C. Boehm, S.M. Fier-Thompson, J.W. Abt, M.E. Soreson, J.M. Smietana, R.F. Hall, R.S. Garigipati, P.E. Bender, K.F. Erhard, A.J. Krog, G.A. Hofmann, P.L. Sheldrake, P.C. McDonnell, S. Kumar, P.R. Young and J.L. Adams, Regulation of stress-induced

- cytokine production by pyridinylimidazoles; inhibition of CSBP kinase, *Bioorg. Med. Chem.* 5 (1997) 49-64.
- [15] A. Shaabani and A. Rahmati, Silica sulfuric acid as an efficient and recoverable catalyst for the synthesis of trisubstituted imidazoles, *J. Mol. Catal. A. Chem.* 249 (2006) 246-248.
- [16] S. Kantevari, S.V.N. Vuppalapati, D. O. Biradar and L. Nagarapu, Highly efficient, one-pot, solvent-free synthesis of tetrasubstituted imidazoles using $\text{HClO}_4\text{-SiO}_2$ as novel heterogeneous catalyst, *J. Mol. Catal. A. Chem.* 266 (2007) 109-113.
- [17] M. Kidwai, P. Mothsra, V. Babsal and R. Goyal, Efficient Elemental Iodine Catalyzed One-Pot Synthesis of 2,4,5-Triarylimidazoles, *Monatsh. Chem.* 137 (2006) 1189-1194.
- [18] L.M. Wang, Y.H. Wang, H. Tian, Y.F. Yao, J.H. Shao and B. Liu, Ytterbium triflate as an efficient catalyst for one-pot synthesis of substituted imidazoles through three-component condensation of benzil, aldehydes and ammonium acetate, *J. Fluorine Chem.* 127 (2006) 1570-1573.
- [19] G.V.M. Sharma, Y. Jyothi and P.S. Lakshmi, An efficient room temperature synthesis of tri- and tetra-substituted imidazoles catalysed by ZrCl_4 , *Synth. Commun.* 36 (2006) 2991-3000.
- [20] S. Balalaie and A. Arabanian, One-pot synthesis of tetrasubstituted imidazoles catalyzed by zeolite HY and silica gel under microwave irradiation, *Green Chem.* 2 (2000) 274-276.
- [21] M. M. Heravi, K. Bakhtiari, H. A. Oskooie and S. Taheri, Synthesis of 2,4,5-triaryl-imidazoles catalyzed by $\text{NiCl}_2 \cdot 6\text{H}_2\text{O}$ under heterogeneous system, *J. Mol. Catal. A. Chem.* 263 (2007) 279-281.
- [22] K. Sivakumar, A. Kathirvel and A. Lalitha, Simple and efficient method for the synthesis of highly substituted imidazoles using zeolite-supported reagents, *Tetrahedron Lett.* 51 (2010) 3018-3021.

- [23] (a) J. F. Hayes, M. B. Mitchell and C. Wicks, A Novel Synthesis of 2,4,5-Triarylimidazoles, *Heterocycles*, 38 (1994) 575-585; (b) L. Revesz, F. Bonne and P. Makavou, Vicinal bromostannanes as novel building blocks for the preparation of di- and trisubstituted imidazoles, *Tetrahedron Lett.* 39 (1998) 5171-5174.
- [24] N.J. Liverton, J.W. Butcher, C.F. Claiborne, D.A. Claremon, B.E. Libby, K.T. Nguyen, S. M. Pitzenberger, H.G. Selnick, G.R. Smith, A. Tebben, J. P. Vacca, S. L. Varga, L. Agarwal, K. Dancheck, A.J. Forsyth, D.S. Fletcher, B. Frantz, W.A. Hanlon, C.F. Harper, S.J. Hofsess, M. Kostura, J. Lin, S. Luell, E.A. O'Neill, C. J. Orevillo, M. Pang, J. Parsons, A. Rolando, Y. Sahly, D.M. Visco and S.J. O'Keefe, Design and synthesis of potent, selective, and orally bioavailable tetrasubstituted imidazole inhibitors of p38 mitogen-activated protein kinase, *J. Med. Chem.* 42 (1999) 2180-2190.
- [25] U. Diebold, The surface science of titanium dioxide, *Surf. Sci. Rep.* 48 (2003) 53-229.
- [26] D.A Tryk, A Fujishima and K Honda, Recent topics in photoelectrochemistry: achievements and future prospects, *Electrochimica Acta.* 45 (2000) 2363-2376.
- [27] L. G. Phillips and D. M. Barbano, The Influence of fat substitutes based on protein and titanium dioxide on the sensory properties of low-fat milks, *J. Dairy Sci.* 80 (1997) 2726-2731.
- [28] J.P. Hewitt, Formulating Water-resistant TiO₂ Sunscreens, *Cosmet. Toiletries*, 114 (1999) 59-63.
- [29] G. Palmisano, V. Augugliaro, M. Pagliaro and L. Palmisano, Photocatalysis: a promising route for 21st century organic chemistry, *Chem. Commun.* (2007) 3425-3437.
- [30] M. Mahalakshmi, B. Arabindoo, M. Palanichamy and V. Murugesan, Photocatalytic degradation of carbofuran using semiconductor oxides, *J. Hazard. Mater.* 143 (2007) 240-245.

- [31] M. Abu Tariq, M. Faisal and M. Muneer, Semiconductor-mediated photocatalysed degradation of two selected azo dye derivatives, amaranth and bismarck brown in aqueous suspension, *J. Hazard. Mater.* 127 (2005) 172-179.
- [32] O. S. Mohamed, A.E-A.M. Gaber and A.A. Abdel-Wahab, Photocatalytic oxidation of selected aryl alcohols in acetonitrile, *J. Photochem. Photobiol. A.* 148 (2002) 205-210.
- [33] H. Sharghi and M. Hosseini Sarvari, TiO₂ Catalysed One Step Beckmann Rearrangement of Aldehydes and Ketones in Solvent Free Conditions, *J. Chem. Res. (S)*. (2003) 176.
- [34] M.A. Pasha, K. Manjula and V.P. Jayashankara, Titanium Dioxide-Mediated Friedel-Crafts Acylation of Aromatic Compounds in Solvent-Free Condition under Microwave Irradiation, *Synth. React. Inorg. Met. Org. Chem.* 36 (2006) 321-324.
- [35] S. Kumari, A. Shekhar and D.A D. Pathak, Ultrasound-Promoted Synthesis of 9-Aryl-1,8-dioxooctahydroxanthenes Using TiO₂ as a Cheap and Reusable Catalyst, *Chem. Sci. Trans.* 3 (2) 3 (2) (2014) 652-663.
- [36] K. V. Subba Rao, B. Srinivas, A. R. Prasad and M. Subrahmanyam, A novel one step photocatalytic synthesis of dihydropyrazine from ethylenediamine and propylene glycol, *Chem. Commun.* (2000) 1533-1534.
- [37] K. V. Subba Rao and M. Subrahmanyam, Synthesis of 2-methylpiperazine by photocatalytic reaction in a non-aqueous suspension of semiconductor-zeolite composite catalysts, *Photochem. Photobiol. Sci.* 1 (2002) 597-599.
- [38] (a) V. Jeena and R. S. Robinson, Green oxidations: Titanium dioxide induced tandem oxidation coupling reactions, *Beilstein J. Org. Chem.* 10 (2014) 1524-1535; (b) X. J. Lang, H. W. Ji, C. C. Chen, W. H. Ma and J. C. Zhao, Selective formation of imines by aerobic photocatalytic oxidation of amines on TiO₂, *Angew. Chem. Int. Ed.* 50 (2011) 3934-3937.

- [39] G. Brahmachari, S. Das, A simple and straightforward method for one-pot synthesis of 2,4,5-triarylmidazoles using titanium dioxide as an eco-friendly and recyclable catalyst under solvent free conditions, *Ind. J. Chem.* 52B (2013) 387-393
- [40] Q. Huang and L. Zhang, Preparation, chain conformation and anti-tumor activities of water-soluble phosphated (1 → 3)- α - d-glucan from *Poria cocos* mycelia, *Carbohydr. Polym.* 83 (2011) 1363-1369.
- [41] R. Weissleder, A. Bogdanov, E.A. Neuwelt and M. Papisov, Long-circulating iron oxides for MR imaging, *Adv. Drug. Deliv. Rev.* 16 (1995) 321-334.
- [42] A.P. Fink, M. Chastellain, L.J. Jeanneret, A. Ferrari and H. Hofmann, Development of functionalized superparamagnetic iron oxide nanoparticles for interaction with human cancer cells, *Biomater.* 26 (2005) 2685-2694.
- [43] S.T. Bae, S.W. Lee and Y. Takemura, Applications of NiFe₂O₄ nanoparticles for a hyperthermia agent in biomedicine, *Appl. Phys. Lett.* 89 (2006) 252503-252505.
- [44] X. Zhao, R.T. Dytico, K. Wang and W. Tan, Collection of trace amounts of DNA/mRNA molecules using genomagnetic nanocaptors, *Anal. Chem.* 75 (2003) 3476-3483.
- [45] A.S. Lubbe, C. Alexiou and C. Bergemann, Clinical Applications of Magnetic Drug Targeting, *J. Surg. Res.* 95 (2001) 200-206.
- [46] C. Xu, K. Xu, H. Gu, X. Zhong, Z. Guo, R. Zheng, X. Zhang and B. Xu, Nitrioltriacetic Acid-Modified Magnetic Nanoparticles as a General Agent to Bind Histidine-Tagged Proteins, *J. Am. Chem. Soc.* 126 (2004) 3392-3393.
- [47] H. Xu, N. Tong, L. Cui, Y. Lu and H. Gu, Preparation of hydrophilic magnetic nanospheres with high saturation magnetization, *J. Magn. Magn. Mater.* 311 (2007) 125-130.

- [48] (a) M. Marinescu, M. Langer, A. Durand, C. Olivier, A. Chabrol, H. Rositi, F. Chauveau, T.H. Cho, N. Nighoghossian, Y. Berthezène, F. Peyrin and M. Wiart, Synchrotron radiation X-ray phase micro-computed tomography as a new method to detect iron oxide nanoparticles in the Brain, *Mol. Imaging Biol.* 15(5) (2013) 552-559; (b) M. Shao, L. Yan, H. Pan, I.Ivanov and Bin Hu, Giant Magnetic Field Effects on Electroluminescence in Electrochemical Cells, *Adv. Mater.* 23 (2011) 2216–2220; (c) Y. Xie, M.Gong, T.A. Shastry, J. Lohrman, M. C. Hersam and S. Ren, Broad-Spectral-Response Nanocarbon Bulk-Heterojunction Excitonic Photodetectors, *Adv. Mater.* 25 (2013) 3433–3437; (d) H. B. Radousky and H. Liang, Energy harvesting: an integrated view of materials, devices and applications, *Nanotechnology*, 23 (2012) 502001-502036.
- [49] (a) J. Jayabharathi, V. Thanikachalam, V. Kalaiarasi and K. Jayamoorthy, Intramolecular excited charge transfer, radiative and radiationless charge recombination processes in donor–acceptor imidazole derivatives, *J. Photochem. Photobiol. A.* 275 (2014) 114-126; (b) J. Jayabharathi, V. Thanikachalam, V. Kalaiarasi and K. Jayamoorthy, Optical properties of 1-(4,5-diphenyl-1-p-tolyl-1H-imidazol-2-yl)naphthalen-2-ol – ESIPT process, *Spectrochim. Acta, Part A.* 120 (2014) 389-394; (c) C. Karunakaran, J. Jayabharathi, V. Kalaiarasi and K. Jayamoorthy, Enhancing photoluminescent behavior of 2-(naphthalen-1-yl)-1,4,5-triphenyl-1H-imidazole by ZnO and Bi₂O₃, *Spectrochim. Acta, Part A.* 118 (2014) 182-186; (d) J. Jayabharathi, V. Kalaiarasi, V. Thanikachalam and K. Jayamoorthy, Dynamics of solvent controlled ESIPT of π -expanded imidazole derivatives - pH effect, *J. Fluoresc.* 24 (2014) 625-637; (e) J. Jayabharathi, V. Thanikachalam, P. Ramanathan and A. Arunpandiyam, Intramolecular excited proton transfer of 1-(1-phenyl-1H-phenanthro[9,10-d]imidazol-2-yl)naphthalen-2-ol – A combined experimental and Quantum chemical studies, *Spectrochim. Acta, Part*

- A. 121 (2014) 551-558; (f) J. Jayabharathi, P. Ramanathan, V. Thanikachalam and A. Arunpandiyan, Kamlet-Taft and Catalan solvatochromism of some π -expanded phenanthrimidazole derivatives – DFT analysis, *Spectrochim. Acta, Part A.* 133 (2014) 201-206; (g) J. Jayabharathi, C. Karunakaran, V. Thanikachalam and P. Ramanathan, Binding and fluorescence enhancing behaviour of phenanthrimidazole with different phases of TiO₂, *New J. Chem.* 38 (2014) 4321-4335; (h) V. Thanikachalam, A. Arunpandiyan, J. Jayabharathi and P. Ramanathan, Photophysical properties of the intramolecular excited charge-transfer states of π -expanded styryl phenanthrimidazoles – Effect of solvent polarity, *RSC adv.* 4 (2014) 6790-6806.
- [50] Gaussian 03, Revision C.02, M. J. Frisch, G. W. Trucks, H. B. Schlegel, G. E. Scuseria, M. A. Robb, J. R. Cheeseman, J. A. Montgomery, Jr., T. Vreven, K. N. Kudin, J. C. Burant, J. M. Millam, S. S. Iyengar, J. Tomasi, V. Barone, B. Mennucci, M. Cossi, G. Scalmani, N. Rega, G. A. Petersson, H. Nakatsuji, M. Hada, M. Ehara, K. Toyota, R. Fukuda, J. Hasegawa, M. Ishida, T. Nakajima, Y. Honda, O. Kitao, H. Nakai, M. Klene, X. Li, J. E. Knox, H. P. Hratchian, J. B. Cross, V. Bakken, C. Adamo, J. Jaramillo, R. Gomperts, R. E. Stratmann, O. Yazyev, A. J. Austin, R. Cammi, C. Pomelli, J. W. Ochterski, P. Y. Ayala, K. Morokuma, G. A. Voth, P. Salvador, J. J. Dannenberg, V. G. Zakrzewski, S. Dapprich, A. D. Daniels, M. C. Strain, O. Farkas, D. K. Malick, A. D. Rabuck, K. Raghavachari, J. B. Foresman, J. V. Ortiz, Q. Cui, A. G. Baboul, S. Clifford, J. Cioslowski, B. B. Stefanov, G. Liu, A. Liashenko, P. Piskorz, I. Komaromi, R. L. Martin, D. J. Fox, T. Keith, M. A. Al-Laham, C. Y. Peng, A. Nanayakkara, M. Challacombe, P. M. W. Gill, B. Johnson, W. Chen, M. W. Wong, C. Gonzalez, and J. A. Pople, Gaussian, Inc., Wallingford CT, 2004.
- [51] (a) J. Nikkanen, T. Kanerva and T. Ma'ntyla, The effect of acidity in low-temperature synthesis of titanium dioxide, *J. Cryst. Growth.* 304 (2007) 179-183; (b) H. Cheng, J.

- Ma, Z. Zhao and L. Qi, Hydrothermal Preparation of Uniform Nanosize Rutile and Anatase Particles, *Chem. Mater.* 7 (1995) 663-671; (c) A. M. Smith and S. Nie, Semiconductor nanocrystals: structure, properties, and band gap engineering, *Accounts of Chemical Research*, 2010, 43, 190-200.
- [52] C. Karunakaran and P. Gomathisankar, Solvothermal synthesis of CeO₂-TiO₂ nanocomposite for visible light-photocatalytic detoxification of cyanide, *ACS Sustainable Chem. Eng.* 1 (2003) 1549-1555.
- [53] (a) R. Singh, A. Karmakar, J. S. Manna, D. Das and M. K. Mitra, Electronic interaction between Mg porphyrin and TiO₂ within a conducting brain like polypyrrole nanomatrix, *Procedia Materials Science*, 6 (2014) 762 -769; (b) B.M. Wepster, in: W. Klyne and P.D.B. dela Mare Eds., *Progress in Stereochemistry*, Academic Press, New York, vol. 2 (1958) ch. 4.
- [54] J.K. Dey and S.K. Dogra, Absorption and fluorescence characteristics of 2-alkyl and 2-arylbenzoxazoles in different solvents and at various acid concentrations, *Ind. J. Chem.* 29A (1990) 1153.
- [55] J.K. Dey and S.K. Dogra, Dual Fluorescence of 2-[4-(Dimethylamino)phenyl] benzothiazole and Its Benzimidazole Analog: Effect of Solvent and pH on Electronic Spectra, *J. Phys. Chem.* 98 (1994) 3638-3644.
- [56] J.K. Dey and S.K. Dogra, Solvatochromism and Prototropism in 2-(Aminophenyl) Benzothiazoles, *Bull. Chem. Soc. Jpn.* 64 (1991) 3142-3152.
- [57] S.K. Dogra, Intra- and intermolecular proton transfer reactions in 2-phenyl substituted benzazoles, *Proc. Indian Acad. Sci.* 104 (1992) 635-647.
- [58] J.F. Ireland and P.A.H. Wyatt, Acid-Base Properties of Electronically Excited States of Organic Molecules, *Adv. Phys. Org. Chem.* 12 (1976) 131-160.

- [59] G. Krishnamoorthy and S.K. Dogra, Dual fluorescence of 2-(4'-*N,N*-dimethylaminophenyl)benzoxazole: effect of solvent and pH, Chem. Phys. 243 (1999) 45–59.

Figure captions

Figure 1. (a) Powder X-ray diffraction (XRD) pattern of PSIMN; (b) TEM image of PSIMN

Figure 2. VSM spectra of (a) Cubic Fe₂O₃; (b) PSIMN

Figure 3. Attachment of phosphated imidazole to Fe₂O₃

Figure 4. Absorption (a) and emission (b) spectra of CPPIVI, PSI and PSIMN

Figure 5. Life time spectra of CPPIVI, PSI and PSIMN

Figure 6. Protonation of (E)-4-(2-(1-(4-chlorophenyl)-1H-phenanthro[9,10-d]imidazol-2-yl)vinyl)-N,N-dimethylaniline (CPPIVI).

Figure 7. Absorption (a) and emission (b) spectra of the prototropic species of (E)-4-(2-(1-(4-chlorophenyl)-1H-phenanthro[9,10-d]imidazol-2-yl)vinyl)-N,N-dimethylaniline (CPPIVI)

Figure S1. (a) X-ray diffraction pattern (XRD) of TiO₂ (R); (b) SEM image of TiO₂ (R)

Figure S2. (a) Diffused reflectance spectra of TiO₂ (R); (b) Solid state photoluminescence spectra of TiO₂ (R)

Figure S3. Possible mechanism for catalytic synthesis of phenanthrimidazoles

Figure S4. Reusability of TiO₂ (R) for catalytic synthesis of phenanthrimidazoles

Figure S5. SEM images of (a) PSIMN; (b) PSI

Figure S6. EDX spectra of (a) PSIMN; (b) PSI

Figure S7. Fourier transform infrared spectra of (a) CPPIVI; (b) Phosphated styrylimidazole; (c) PSIMN; (d) Fe₂O₃ nanoparticles

Figure S8. Energetic positions of CPPIVI, PSI and PSIMN

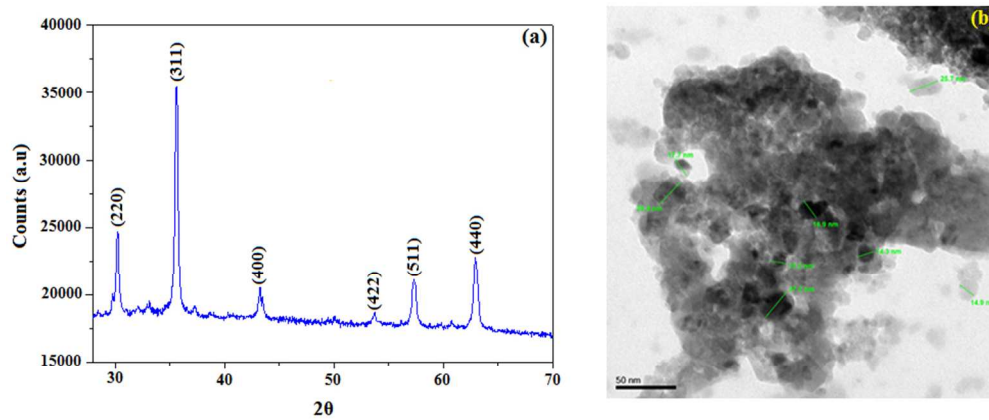


Figure 1

259x119mm (96 x 96 DPI)

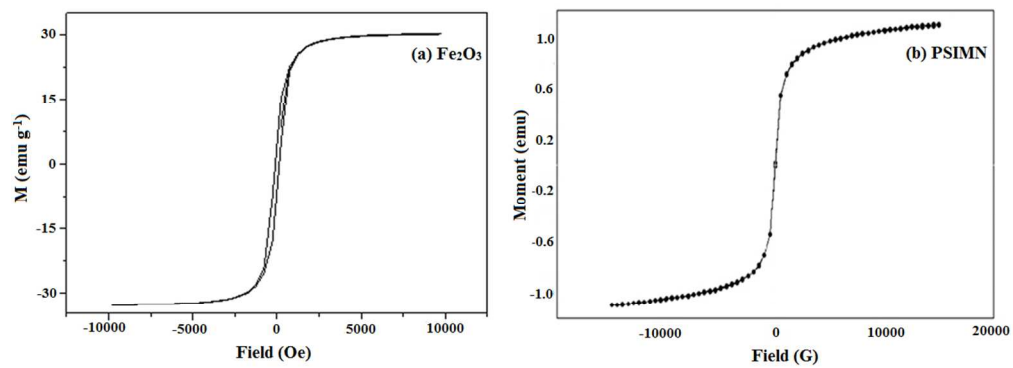
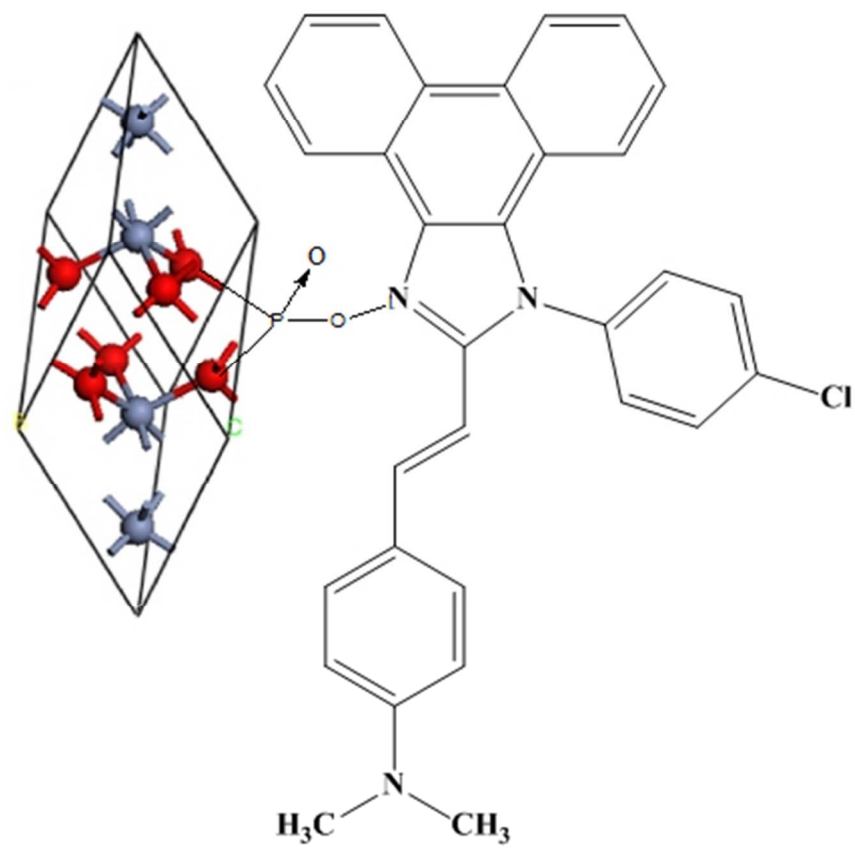


Figure 2

202x81mm (150 x 150 DPI)

**Figure 3**

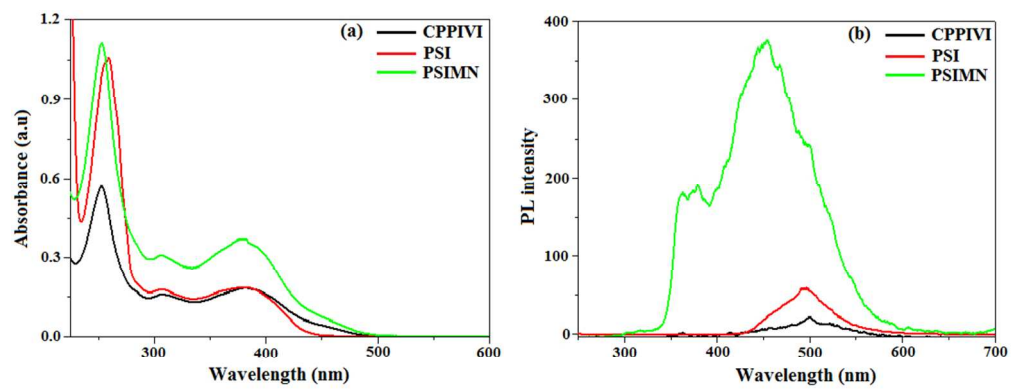


Figure 4

290x125mm (96 x 96 DPI)

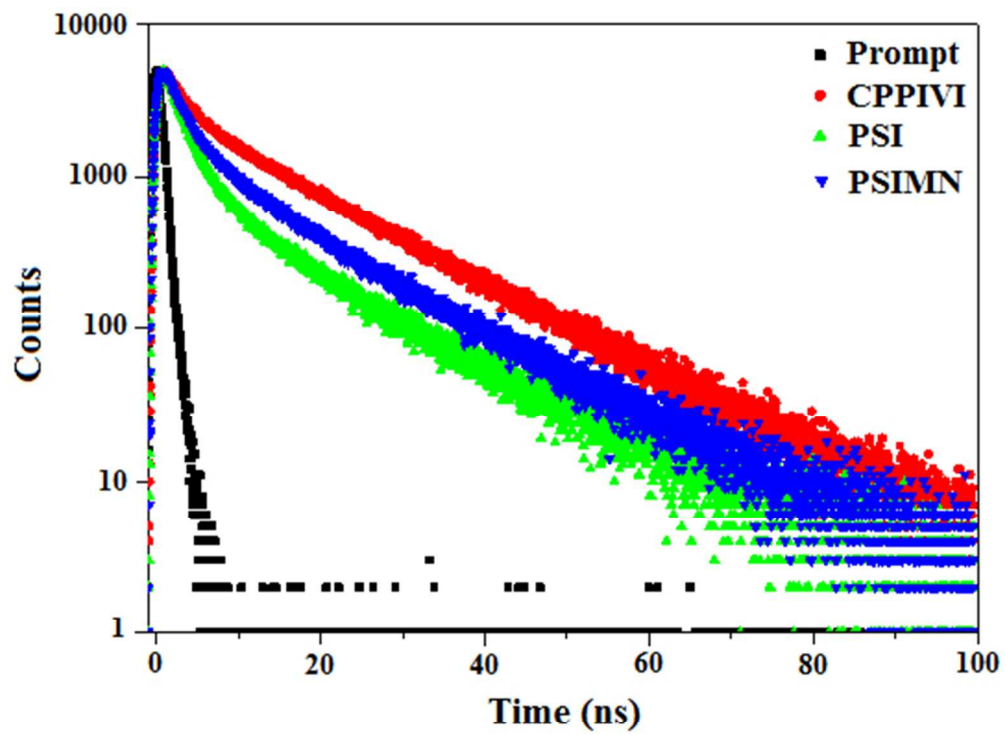


Figure 5

143x117mm (96 x 96 DPI)

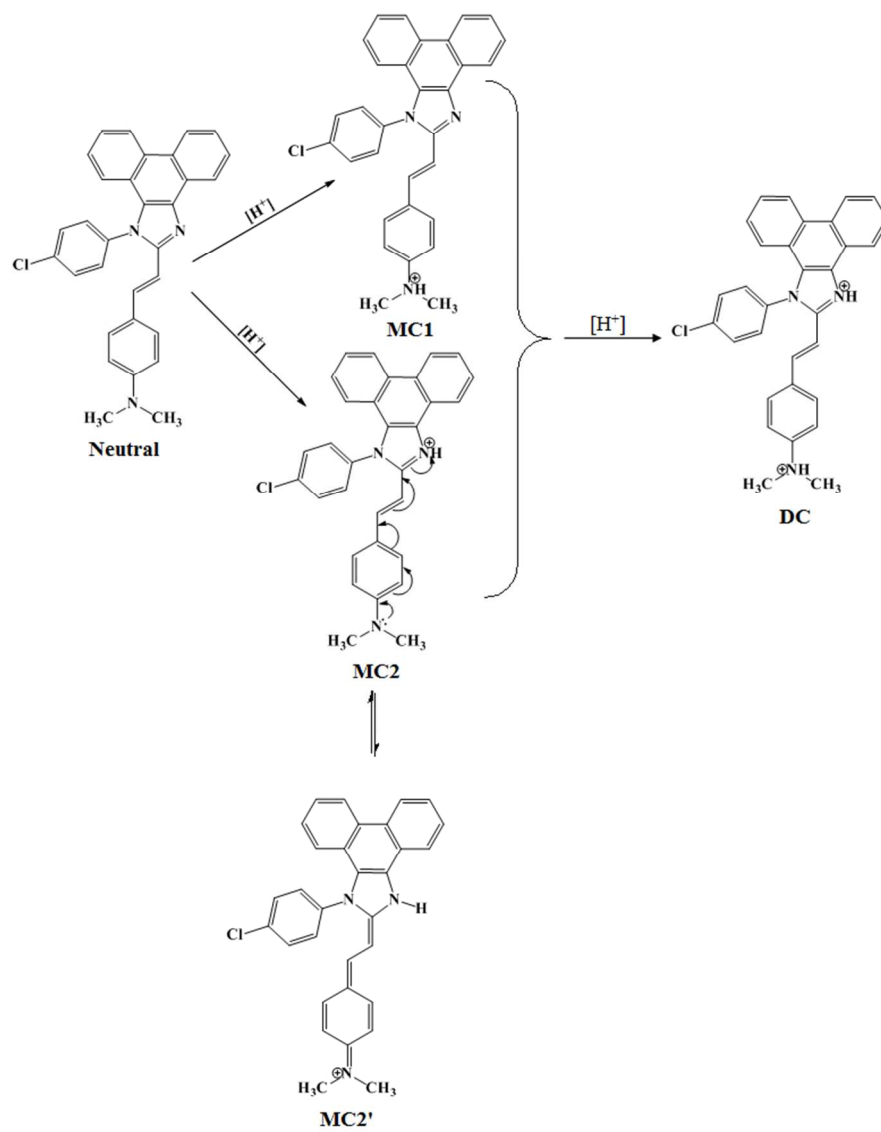


Figure 6

208x280mm (96 x 96 DPI)

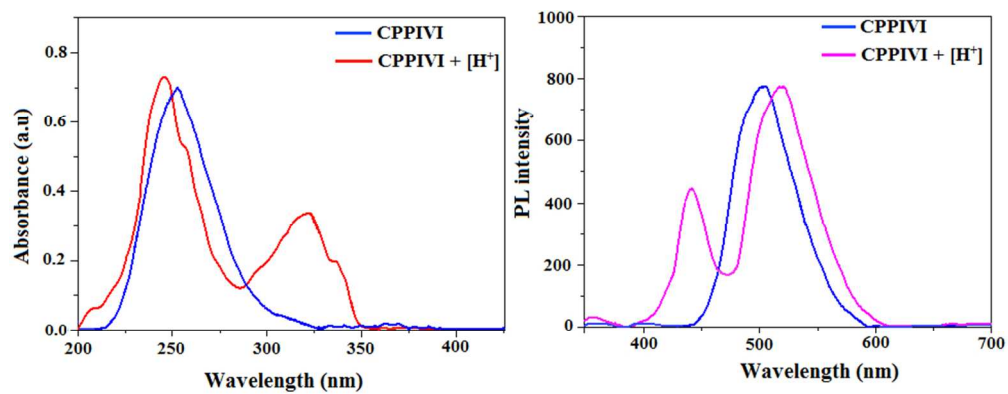


Figure 7

256x109mm (96 x 96 DPI)

Table 1. IR data of CPPIVI, PSI and PSIMN

Bonding	CPPIVI	PSI	PSIMN	Fe₂O₃
C=N	1601	1620	1650	-
NH-CH	3424	3381	3375	-
Aromatic C-C Str.	1540, 1524, 1496, 1453	-	-	-
C-H Bending	803, 748, 738, 722	818, 755	820, 755	-
Fe – O	-	-	1647	1631
PO ₄ ⁻³	-	1080	1099	-

Table 2. Bi exponential fitting parameter for fluorescence decay of CPPIVI, PSI and PSIMN

Compound	a_1	τ_1 (ns)	a_2	τ_2 (ns)	τ_{ave} (ns)	k_r $\times 10^{-8} s^{-1}$	k_{nr} $\times 10^{-8} s^{-1}$	E%	k_{et} $\times 10^{-8} s^{-1}$
CPPIVI	1.9899×10^{-2}	2.1862×10^{-9}	1.4771×10^{-2}	1.4668×10^{-8}	7.50	0.65	0.70	-	-
PSI	6.1264×10^{-2}	2.7745×10^{-9}	9.6601×10^{-3}	1.4392×10^{-8}	4.36	1.10	1.20	-	-
PSIMN	3.1373×10^{-2}	2.3905×10^{-9}	1.1147×10^{-2}	2.3905×10^{-9}	5.23	0.95	0.91	30.3	0.58

Table 3. Absorption ($\lambda_{\text{max}}^{\text{ab}}$, nm), absorbance (A), emission ($\lambda_{\text{max}}^{\text{fl}}$, nm) and fluorescence quantum yield (ϕ_{fl}) of different prototropic species of CPPIVI in different solvents

Species	$\lambda_{\text{max}}^{\text{ab}}$	A ^a	$\lambda_{\text{max}}^{\text{fl}}$	ϕ_{fl}
Cyclohexane				
CPPIVI [0.04 M TFA]	253	1.49	501	0.59
MC1 [0.04 M TFA]	243	0.50	440	-
MC2 [0.04 M TFA]	340	1.30	520	0.32
Dichloromethane				
CPPIVI [0.0 M H ₂ SO ₄]	248	1.43	486	0.50
MC1 [0.06 M H ₂ SO ₄]	241	0.53	421	0.29
MC2 [0.06 M H ₂ SO ₄]	282	0.80	493	-
DC [1.2 M H ₂ SO ₄]	245	0.61	392	-
Water				
CPPIVI	243	1.24	429	0.47
MC1 [pH 0.3]	241	0.61	423	0.07
MC2 [pH 0.3]	282	0.18	462	-
DC [H ₀ - 4.0]	245	0.60	439	0.23

Table 4. Total energy (E, eV), dipole moment (μ , D), dihedral angles (ϕ°) & (θ°) and atomic charges $P(r)$ for the MC1, MC2 and DC of CPPIVI

Parameters	Neutral	MC1	MC2	DC
ϕ	0.30	5.20	2.10	5.20
Θ	5.98	98	0.58	120
μ	0.92	15.1	3.01	11.10
E	-1589.20	-2015.20	-1631.89	-2198.12
$P(r)N17$	-0.1561	0.3921	0.1323	-0.0100
$P(r)N61$	-0.2012	0.1813	-0.0201	0.2515

Table of contents (TOC)

